(12) INTERNATIONAL APPLICATION PUBLISHED UNDER THE PATENT COOPERATION TREATY (PCT)

(19) World Intellectual Property Organization
International Bureau

(43) International Publication Date
7 June 2012 (07.06.2012)

WIPO | PCT

(10) International Publication Number
WO 2012/073009 A2

(51) International Patent Classification:
B81C 1/00 (2006.01)

(21) International Application Number:
PCT/GB2011/052344

(22) International Filing Date:
28 November 2011 (28.11.2011)

(25) Filing Language: English

(26) Publication Language: English

(30) Priority Data:
1020503.7 3 December 2010 (03.12.2010) GB

(71) Applicant *(for all designated States except US)*: **IMPERIAL INNOVATIONS LIMITED** [GB/GB]; 52 Princes Gate, South Kensington, London Greater London SW7 2PG (GB).

(72) Inventors; and

(75) Inventors/Applicants *(for US only)*: **ALBRECHT, Tim** [DE/GB]; Ground Floor Flat, 27 Charleville Road, London Greater London W14 9JJ (GB). **IVANOV, Aleksandar Petrov** [BG/GB]; Flat 156, 3 Cornell Square, London Greater London SW8 2ES (GB). **EDEL, Joshua Benno** [GB/GB]; 104 Green Lane, Edgware, London Greater London HA8 8EJ (GB).

(74) Agent: **Barker Brettell LLP**; 100 Hagley Road, Edgbaston, Birmingham West Midlands B16 8QQ (GB).

(81) Designated States *(unless otherwise indicated, for every kind of national protection available)*: AE, AG, AL, AM, AO, AT, AU, AZ, BA, BB, BG, BH, BR, BW, BY, BZ, CA, CH, CL, CN, CO, CR, CU, CZ, DE, DK, DM, DO, DZ, EC, EE, EG, ES, FI, GB, GD, GE, GH, GM, GT, HN, HR, HU, ID, IL, IN, IS, JP, KE, KG, KM, KN, KP, KR, KZ, LA, LC, LK, LR, LS, LT, LU, LY, MA, MD, ME, MG, MK, MN, MW, MX, MY, MZ, NA, NG, NI, NO, NZ, OM, PE, PG, PH, PL, PT, QA, RO, RS, RU, RW, SC, SD, SE, SG, SK, SL, SM, ST, SV, SY, TH, TJ, TM, TN, TR, TT, TZ, UA, UG, US, UZ, VC, VN, ZA, ZM, ZW.

(84) Designated States *(unless otherwise indicated, for every kind of regional protection available)*: ARIPO (BW, GH, GM, KE, LR, LS, MW, MZ, NA, RW, SD, SL, SZ, TZ,

[Continued on next page]

(54) Title: NANOPORE DEVICES

(57) Abstract: A method of fabricating a nanopore device comprises: providing a layer of substrate material having a pore through it, and depositing a pair of electrodes on the surface of the substrate material such that the electrodes are located adjacent to the pore. The electrodes are deposited by particle beam induced deposition.The deposition may be induced using a particle beam that is non-perpendicular to the surface of the substrate.

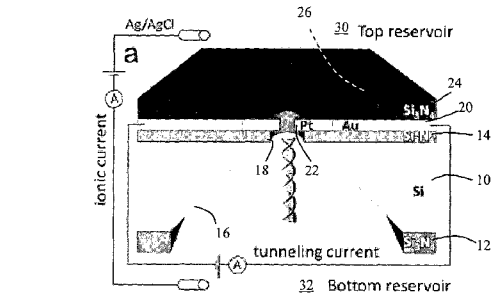

Fig. 1a

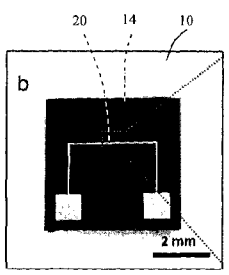

Fig. 1b

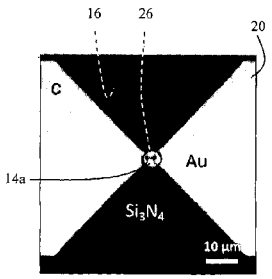

Fig. 1c

WO 2012/073009 A2

UG, ZM, ZW), Eurasian (AM, AZ, BY, KG, KZ, MD, RU, TJ, TM), European (AL, AT, BE, BG, CH, CY, CZ, DE, DK, EE, ES, FI, FR, GB, GR, HR, HU, IE, IS, IT, LT, LU, LV, MC, MK, MT, NL, NO, PL, PT, RO, RS, SE, SI, SK, SM, TR), OAPI (BF, BJ, CF, CG, CI, CM, GA, GN, GQ, GW, ML, MR, NE, SN, TD, TG).

Published:

— *without international search report and to be republished upon receipt of that report (Rule 48.2(g))*

Nanopore Devices

Field of the Invention

The present invention relates to nanopore devices, in particular devices with integrated electrodes. The invention may be used, for example, in the fabrication of a DNA nanopore detector with integrated tunnelling electrodes, or of a dielectrophoretic trap.

Background to the Invention

Nanometer-scale pores (nanopores) can be used as versatile single-molecule sensors for the label-free detection and structural analysis of biological polymers such as DNA, RNA, polypeptides and DNA-protein complexes in solution. In a typical nanopore experiment, biological molecules are electrokinetically driven through a nanopore by an externally applied electric field. This results in a characteristic blockade of the ionic current across the pore. From the ionic current blockade measurements, information on molecular properties such as length, composition, and interactions with other biomolecules can be extracted. When a biological polyelectrolyte such as DNA is driven through a pore with a diameter of a few nanometers, the molecule is unfolded from its coiled state and travels through the pore in a linear configuration. This gives rise to the unique opportunity to directly access the molecular structure of DNA. Unfortunately, the state-of-the-art detection based on ionic current blockade or fluorescence spectroscopy generally lacks the spatial and temporal resolution necessary to obtain structural information at the single base level.

An alternative detection method based on tunnelling transport in DNA (perpendicular to the DNA backbone) has recently been proposed to alleviate these limitations. Due to its quantum mechanical origin, the tunnelling current decays rapidly with distance, leading to enhanced spatial resolution, and also provides molecular specificity. These characteristics form the basis of Scanning Tunnelling Microscopy (STM). Notably, identification of single (bio)molecules, nanoparticles and even single nucleotides with tunnelling currents has been predicted by theoretical work and experimentally by STM.

Very recently, Tsutsui et al. were able to trap and identify single nucleotides between tunnelling electrodes, providing first experimental evidence towards a DNA

sequencing-by-tunnelling technology [Tsutsui, M.; Taniguchi, M.; Yokota, K.; Kawai, T. *Nat. Nanotechnol.* 2010, *5*, 286]. While exceptionally valuable as a proof of principle, these experiments were limited to single nucleotides or performed in a STM environment. A potentially much faster and hence more applicable approach is to fabricate a device that combines a nanopore with a tunnelling junction. In such a configuration, the nanopore is used to "unfold" the DNA strand to a linear configuration, while a tunnelling junction precisely aligned at the pore opening detects sequence-specific changes in the tunnelling current. Unfortunately, while solid-state nanopores and nanogap tunnelling electrodes are routinely fabricated on separate platforms, combining DNA translocation through a pore with concurrent tunnelling and ionic current detection has not previously been realized.

Summary of the Invention

The present invention provides, according to a first aspect, a method of fabricating a nanopore device, the method comprising: providing a layer of substrate material having a pore through it, and depositing a pair of electrodes on the surface of the substrate material such that the electrodes are located adjacent to the pore, wherein the electrodes are deposited by particle beam induced deposition.

The electrodes may be located on opposite sides of the pore, for example if the device only includes two electrodes or if it has four electrodes equally spaced around the pore. In some embodiments there may be an odd number of electrodes, such as three, in which case any pair of the electrodes may not be on opposite sides of the pore.

The device may be a measurement device. For example it may be a tunnelling current measurement device arranged to measure tunnelling current between the electrodes, or it may be another type of device, such as a dielectrophoresis trap in which the potential of the electrodes is arranged to trap a molecule in the pore.

The particle beam used to induce the deposition may, for example, be an electron beam or an ion beam.

At least one, and preferably both, of the electrodes may be deposited so as to partially block the pore. This can help to reduce the size of the pore thereby to restrict the

movement of molecules through the pore. It can also result in a gap between the electrodes which is less than the nominal mean diameter of the pore.

The pore may be a nanopore. For example, the pore may have a mean diameter of 100nm or less.

The electrodes may be deposited so as to leave a gap between them which is small enough for tunnelling current to flow between the electrodes. For example the gap may be 10nm or less, and in some cases 5nm or less.

The deposition may be induced using a particle beam that is non-perpendicular to the surface of the substrate. This can help to form an electrode with a narrow profile and a more pointed tip than if the particle beam is perpendicular to the substrate surface.

For example the deposition may be induced using a particle beam that is at a deposition angle of 80° or less, more preferably 60° or less, to the surface of the substrate.

During the deposition the particle beam may be moved along the substrate in a direction which is non-perpendicular to the beam. This can further contribute to the formation of a narrow electrode. For example the beam may be moved along the substrate in a direction that is on the line of intersection between a plane and the surface of the substrate, the plane being perpendicular to the substrate and parallel to the particle beam.

The pore may be formed by etching, or by a particle beam. The pore and the electrodes may be formed by respective beams of a dual beam or other multibeam apparatus having two particle sources each arranged to direct one of the beams at the substrate. The two particle sources and the substrate may be kept stationary during the process of nanopore and nanoelectrode formation. This helps to ensure alignment between the nanopore and nanoelectrode.

The present invention further provides a micropore device comprising a substrate having a pore through it, and a pair of electrodes formed on the substrate and located

adjacent to the pore, wherein at least one of the electrodes comprises a nanowire formed on the surface of the substrate.

The device may be a measurement device such as a tunnelling current measurement device or a dielctrophoretic confinement device.

The electrodes may define a gap between them of no more than 10nm, preferably not more than 5nm. The nanowire may be at least 40nm long, or in some cases at least 100nm long.

At least one of the electrodes, and in some cases each of the electrodes, may partially block the pore.

The device may comprise a substrate layer, which may be silicon. The substrate layer may have a lower layer, which may be of Si_3N_4, on its bottom surface. The substrate layer may have an upper layer, which may be of Si_3N_4, on its top surface. The substrate layer may have an etched cavity or micropore formed through it. The upper layer may be suspended over the micropore. The upper layer may have a nanopore formed through it, which may be over the micropore. Other shapes of cavity in the silicon substrate can of course be used. A pair of microelectrodes may be formed on the top of the upper layer, for example on opposite sides of the micropore. The microelectrodes may define a gap, for example of about 2μm between them. A further protective layer, for example of Si_3N_4, may be provided over the upper layer, or the microelectrodes, or both. A window may be formed in the protective layer, over at least one of the micropore, the nanopore, and microelectrode electrode gap. Nanoelectrodes, for example of platinum, may be formed on the upper layer between the microelectrodes. Each of the nanoelectrodes may be electrically connected to a respective one of the microelectrodes. The nanoelectrodes may extend towards each other on opposite sides of the nanopore. The nanoelectrodes may be are aligned with each other so that they are in a common straight line. The nanoelectrodes may form a tunnelling junction. Contact pads, which may be also formed from platinum, may be provided, connected to the nanoelectrodes, for example at the outer ends of the nanoelectrodes, to provide good electrical contact between the nanoelectrodes and the microelectrodes. The nanoelectrodes may extend part way across the nanopore so that the gap between them is less than the nominal diameter of the nanopore.

Fabrication of a number of a device may include providing a silicon chip, for example of 10 of 300μm thickness. The upper layer, for example of Si_3N_4, may be deposited by Low Pressure Chemical Vapor Deposition (LPCVD). The lower layer may be deposited in the same manner on the opposite face of the bare silicon wafer. The microelectrodes may be formed from gold, for example around 50nm thick. The may be adhered to the upper layer by means of an adhesion layer, for example of chromium. They may be fabricated by conventional optical lithography on the front face of the wafer. A gap, for example of 2μm, may be defined between the tips of the microelectrodes. An additional protective layer, for example of Si_3N_4, may be deposited by Plasma Enhanced Chemical Vapor Deposition (PECVD). A window may be formed, centered at the microelectrode tips, in the protective layer. The additional layer can reduce the membrane capacitance and Faradaic currents by minimizing the electroactive area. A window in the lower layer on the back face of the wafer may be opened, for example by Reactive Ion Etching (RIE). The silicon may be wet etched, for example in KOH solution, to form the micropore. This may leave a freestanding membrane, formed from part of the upper layer aligned to the microelectrodes. The nanopore may then be formed through the membrane. The nanoelectrodes may be formed on the membrane, for example so that they each have one end connected to a respective one of the microelectrodes and the other end overhanging the edge of the nanopore.

Fabrication of the nanopores and/or the nanoelectrodes may be performed using a dual beam Focused Ion Beam (FIB) / Scanning Electron Microscope (SEM) instrument. This can allow for the entire fabrication and alignment process to be controlled *in situ* and monitored in real time. This instrument may comprise an electron gun arranged to generate a beam of electrons. It may also comprise deflector electrodes. It may also comprise a controller arranged to control the electron gun, and optionally to control the potential of the deflector electrodes. This may control the direction of the electron beam. Detectors may be are arranged to detect scattered electrons and electromagnetic radiation to form an image. An ion source may be arranged to generate an ion beam. A further set of deflector electrodes may be arranged to control the direction of the ion beam, for example under control of the controller. A support, which may be in the form of A sample table, may be located at the point of convergence of the electron beam and ion beam. This can be so that a sample can be supported on it and the electron and ion beams directed at it. The sample table may be adjustably mounted so

that the orientation of the table, and hence of the sample can be adjusted. The sample table may be adjustable so that the position of the sample can be adjusted in three dimensions. The position and/or orientation of the sample table may be controlled by the controller. This may allow the controller to control the relative positions of the electron and ion beams, for example by controlling either the direction of the beams, or the position of the sample table, or both. The sample table may be housed within a sealed chamber so that the sample can be immersed in a precursor gas to enable Electron Beam Induced Deposition (EBID).

A single pore may be milled into the membrane, for example between the two microelectrodes, e.g. by FIB milling. This milling may be performed with the membrane having its surface perpendicular to the ion beam. The nanopore may be drilled through the membrane in the direction perpendicular to its upper and lower surfaces.

For the fabrication of the nanoelectrodes, the controller may be controlled by defining a template, which defines a nominal end position for each of the nanoelectrodes, and may thereby define a nominal gap between them. However, lateral broadening of the metal deposit during EBID has to be taken into account, which decreases the actual nanogap size compared to the nominal size as defined in the design template which is used by the controller to control the position of the electron beam. The geometry of the nanogap can be further optimized by performing the deposition at a non-perpendicular angle between the electron beam and the surface of the membrane. The design template which is used to control the movement of the electron beam across the membrane may define the path followed by the centre of the circular area over which the beam impacts the substrate if the beam is perpendicular to the substrate. However, the instrument may not be accurate enough to allow the template to define an electrode shape and position such that the nanoelectrodes are separated by a small enough gap. Therefore the deposition angle of may be controlled and selected so as to provide a gap of the desired width, which may be smaller than the smallest gap size that can be defined by the template. The electron beam may be arranged to hit, at any given time, an oval impact area on the membrane. This may spread more broadly in one direction than a perpendicular direction. For example it may spread more broadly in the direction in which the electron beam is moved across the membrane, which may be the direction in which the nanowire is drawn. The nanoelectrodes produced may be

the same width as, or narrower than, those with a 90° deposition angle. The electrodes may extend further from the end point of the template line in the direction of movement of the electron beam than those produced with a 90° deposition angle. The shape of the impact area of the beam on the substrate may not be a precise oval, but the inclination of the beam will generally mean that the impact area is wider in one direction than in a second perpendicular direction. This direction can be on the line of intersection between a plane and the surface of the substrate, the plane being perpendicular to the substrate and parallel to, or containing, the electron beam.

Some embodiments of the invention can provide a simple but powerful approach to fabricate tunnelling junctions aligned to a nanopore. Proof-of-principle experiments using embodiments of the invention have demonstrated simultaneous detection of DNA translocations using both tunnelling and ionic currents in a nanopore platform. It should be noted that there have been previous reports on the fabrication of nanopores and nanofluidic devices with integrated transverse electrodes; however, in all these cases either the electrode gaps were large or were not used for the detection of analyte. In experiments using embodiments of the invention we were able to fabricate electrode junctions with gap sizes sufficiently small to allow for tunnelling transport to occur, and precisely align the electrode junction to a nanopore for use in DNA translocation experiments.

Functional tunnelling devices according to the invention were identified by tunnelling spectroscopy in different solvents and then used in proof-of-principle experiments demonstrating, for the first time, concurrent tunnelling detection and ionic current detection of DNA molecules in a nanopore platform. This is an important step towards ultra-fast DNA sequencing by tunnelling.

Embodiments of the invention can be used for the detection or characterization of other molecules, such as proteins, polypeptides, or any other biological or non-biological molecules or particles that can be transported through a nanopore.

The present invention may further comprise any one or more features of the preferred embodiments, which will now be described by way of example only with reference to the accompanying drawings.

Brief Description of the Drawings

Figure 1a is a schematic of a nanopore/nanogap device integrated into an electrochemical cell according to an embodiment of the invention;

Figure 1b is an optical image of a 5 mm x 5 mm chip used in the fabrication of the device of Figure 1a;

Figure 1c is an image of a freestanding 40 μm x 40 μm Si3N4 membrane aligned to Au microelectrodes in the chip of Figure 1b;

Figure 1d is an SEM image of a window in a PECVD Si3N4 layer opened by RIE, in the chip of Figure 1b;

Figure 1e is an SEM image of Pt nanoelectrodes fabricated by EBID onto the chip of Figure 1b;

Figure 1f is a magnified SEM image showing the nanopore aligned to the Pt nanoelectrodes of the device of Figure 1e;

Figure 2a is a schematic of a dual beam focused ion beam (FIB)/scanning electron microscope (SEM) used to fabricate the device of Figure 1a;

Figure 2b is a diagram showing the effect of electron beam angle on deposited electrode shape;

Figure 3 is a graph of ionic current through a pore (in 0.1 M KCl) without and with the deposition of the nanowire electrodes;

Figure 4 is a graph of effective pore diameter for 10 typical devices before (1-5) and after (6-10) nanoelectrode fabrication as calculated from ionic current conductance and as measured using SEM data;

Figure 5 is a graph showing nanogap tunnelling current *I-V* curves for nanogaps of various sizes and two controls;

Figure 6 is a set of graphs showing the results of tunnelling spectroscopy performed in air, *n*-hexane, DMSO and 0.1 M NaClO4 for three different devices with a nanogap (a-c) and a single nanowire (d);

Figure 7 is a set of plots of ionic and tunnelling currents as a function of time during events detected with the electrodes/nanopore architecture in an electrolyte solution of 1M KCl, Tris-HCl EDTA buffer, Et = 0.3 V and Ei = -0.8 V.

Description of the Preferred Embodiments

Referring to Figure 1a, a nanopore device according to an embodiment of the invention comprises a silicon substrate layer 10 which is 300μm thick with a lower Si_3N_4 layer 12 on its bottom surface and an upper Si_3N_4 layer 14 on its top surface. The silicon substrate 10 has an etched cavity or micropore 16 formed through it. The upper Si_3N_4 layer 14 is suspended over the micropore 16 and has a nanopore 18 with diameter of about 50nm formed through it at the centre of the micropore 16. Other shapes of cavity in the silicon substrate 10 can of course be used. A pair of gold microelectrodes 20 are formed on the top of the upper Si_3N_4 layer 14 on opposite sides of the micropore 16 with a gap of about 2μm between them. A further protective layer 24 of Si_3N_4 is provided over the upper Si_3N_4 layer 14 and the microelectrodes 20, with a window 26 in it over the micropore 16, nanopore 18 and microelectrode electrode gap. Platinum nanoelectrodes 22 are formed on the upper Si_3N_4 layer 14 between the microelectrodes 20. Each of the nanoelectrodes 22 is electrically connected to a respective one of the microelectrodes 20 and the nanoelectrodes 22 extend towards each other on opposite sides of the nanopore 18. The nanoelectrodes 22 are aligned with each other so that they are in a common straight line and form a tunnelling junction. Contact pads 23 also formed from platinum are provided at the outer ends of the nanoelectrodes 22 to provide good electrical contact between the nanoelectrodes and the microelectrodes 20. The nanoelectrodes extend part way across the nanopore 18 so that the gap between them is less than the nominal diameter of the nanopore, and in this case is of the order of 5nm.

As also shown in Figure 1a, the device can be tested by placing it between a top reservoir 30 and a bottom reservoir 32 so that the nanopore 18 connects the two reservoirs 30, 32. The tunnelling junction formed by the nanoelectrodes 22 is located at the exit, which is the top end in this arrangement, of the nanopore; DNA is inserted in the bottom reservoir and electrophoretically driven through the nanopore and the tunnelling junction. An ionic current detection system comprises two electrodes 34, 36, one in each of the reservoirs 30, 32, connected to a voltage supply 38 with a variable voltage and a current sensor 40 arranged to measure the ionic current flowing between the electrodes 30, 32 through the liquid in the reservoirs. Also the microelectrodes 20 are connected to a tunnelling current detection system which also

comprises a variable voltage supply 42 connected between the microelectrodes 20 and a current sensor 44 arranged to measure the tunnelling current flowing across the nanopore 18 between the nanoelectrodes 22.

In a modification to this embodiment the system can be used as a dielectrophoretic trap. In this case the electrodes 34, 36 are used to measure the ionic current through the nanopore 18 and the potential of the nanoelectrodes 22 is controlled to trap molecules in the nanopore 18.

Fabrication of a number of devices as shown in Figure 1a was started with a 5mm x 5mm silicon chip 10 of 300μm thickness. Si_3N_4 was deposited by Low Pressure Chemical Vapor Deposition (LPCVD) on both faces of the bare silicon wafer to a thickness of 70 nm to form the lower and upper layers 12, 14. The microelectrodes 20 were formed from 50nm thick gold with 10nm chromium adhesion layer and were fabricated by conventional optical lithography on the front face of the wafer 10 with a 2μm gap between the tips of the microelectrodes 20, as shown in Figures 1b and 1c. The additional 300 nm thick protective layer 24 of Si_3N_4 was deposited by Plasma Enhanced Chemical Vapor Deposition (PECVD). A 5μm x 5μm window 26 centered at the microelectrode tips 21 was opened in the PECVD Si_3N_4 layer as shown in Figures 1c and 1d. The additional Si_3N_4 layer 24 reduces the membrane capacitance and Faradaic currents by minimizing the electroactive area. Furthermore, the additional Si_3N_4 layer 24 helps to improve the mechanical strength of the membrane. The window in the LPCVD nitride layer 12 on the back face of the wafer was opened by Reactive Ion Etching (RIE), followed by wet etch of the silicon in KOH solution to form the micropore 16, resulting in a 70 nm thick freestanding Si_3N_4 membrane 14a (40μm x 40μm) aligned to the microelectrodes 20 as shown in Figure 1c and 1d. The nanopore 18 was then formed through the Si_3N_4 membrane 14a, and then the nanoelectrodes formed on the Si_3N_4 membrane 14a so that they each had one end connected to a respective one of the microelectrodes 20 and the other end overhanging the edge of the nanopore 18, as shown in Figures 1e and 1f.

Referring to Figure 2a fabrication of the nanopores 18 and the nanoelectrodes 22 were performed using a dual beam Focused Ion Beam (FIB) / Scanning Electron Microscope (SEM) instrument (Zeiss 1540XB*)*. This allowed for the entire fabrication and alignment process to be controlled *in situ* and monitored in real time. This

instrument comprises an electron gun 50 arranged to generate a beam 52 of electrons and deflector electrodes 54. A controller 56 is arranged to control the electron gun 50 and to control the potential of the deflector electrodes 54 so as to control the direction of the electron beam 52. Detectors 57 are arranged to detect scattered electrons and electromagnetic radiation in known manner to form an image. An ion source 60 is arranged to generate an ion beam 62, and a further set of deflector electrodes 63 is arranged to control the direction of the ion beam 62 under control of the controller 56. A sample table 64 is located at the point of convergence of the electron beam 52 and ion beam 62 so that a sample 66 can be supported on it and the electron and ion beams 52, 62 directed at it. The sample table 64 is adjustably mounted so that the orientation of the table 64, and hence of the sample 66 can be adjusted, and also so that the position of the sample 66 can be adjusted in three dimensions. The position and orientation of the sample table 64 are both controlled by the controller 56. This means that the controller can control the relative positions of the electron and ion beams 52, 62, by controlling either the direction of the beams, or the position of the sample table, or both. The sample table 64 is housed within a sealed chamber 68 so that the sample can be immersed in a precursor gas to enable Electron Beam Induced Deposition (EBID).

Single pores were milled into the Si_3N_4 membrane 14 in between the two Au microelectrodes by FIB milling. This milling was performed with the membrane 14 having its surface perpendicular to the ion beam 62, so that the nanopore 18 was drilled through the Si_3N_4 membrane 14 in the direction perpendicular to its upper and lower surfaces. Pores with diameters of 50 – 80 nm were milled in 2.5 seconds at a beam current of 1 pA. The pore milling process is similar to what has been previously described, for example in Ayub, M.; Ivanov, A.; Hong, J.; Kuhn, P.; Instuli, E.; Edel, J. B.; Albrecht, T. *J. Phys.: Condens. Matter* 2010, *22*, 454128, and Ayub, M.; Ivanov, A.; Instuli, E.; Cecchini, M.; Chansin, G.; McGilvery, C.; Hong, J.; Baldwin, G.; McComb, D.; Edel, J. B.; Albrecht, T. *Electrochim. Acta* 2010, *55*, 8237-8243. Once the pores 18 were milled, the Pt nanoelectrodes 22 were fabricated by Electron Beam Induced Deposition (EBID). In this process, the gaseous methylcyclopentadienyl(trimethyl)Pt precursor is directly injected in the SEM chamber 68 and decomposed by the interaction of the electron beam 52 with the surface of the Si_3N_4 membrane 14. In order to ensure a low material growth rate, the process was carried out at low precursor pressure ($7x10^{-6}$ mbar, base pressure $2x10^{-6}$

mbar). Under these conditions we would expect the deposit to consist of nanometer-sized metal crystals embedded in an amorphous carbon matrix. We determined the conductance of these wires to be 420 nS (*vide infra*), which is sufficient for the present invention.

Finally, for the fabrication of the tunnelling junctions, lateral broadening of the metal deposit during EBID has to be taken into account, which decreases the actual nanogap size compared to the nominal size as defined in the design template which is used by the controller 56 to control the position of the electron beam 52. In this example, electrode junctions deposited with a nominal gap size of 50-60 nm (exposure time: 4 s at 30 kV) exhibited tunnelling behavior. This indicates that the actual gap size is of the order of 5nm or less. The geometry of the nanogap was further optimized by performing the deposition at a non-perpendicular angle, in this case of 54°, between the electron beam 52 and the surface of the membrane 14. Referring to Figure 2b, if the deposition angle is 90° i.e. with the electron beam 52 perpendicular to the surface of the membrane 14, then the electron beam hits an approximately circular area 70 of the membrane 14 and the nanoelectrode is drawn as a nanowire 72. The design template which is used to control the movement of the electron beam across the membrane 14 defines the line to be drawn on the membrane, which is the path 74 followed by the centre of the circular area 70. However, the SEM instrument is not accurate enough to allow the template to define an electrode shape and position such that the nanoelectrodes are separated by a small enough gap. At this deposition angle, the nanoelectrodes 72 produced would not be close enough to each other or close enough to the nanopore 18. Therefore the deposition angle of, in this case 54° was used. Specifically the electron beam makes the deposition angle (of in this case 54°) with the line along the centre of the nanowire electrode. This results in the electron beam 52 hitting, at any given time, an oval impact area 76 on the membrane 14 which spreads more broadly in the direction in which the electron beam 52 is moved and in which the nanowire is drawn. Therefore the nanoelectrodes 78 produced are the same width as, or narrower than, those with a 90° deposition angle, and extend further from the end point of the template line 74 in the direction of movement of the electron beam 52. The shape of the impact area of the beam on the substrate may not be a precise oval, but the inclination of the beam will generally mean that the impact area is wider in one direction than in a second perpendicular direction. If the centre of the beam is moved across the surface of the substrate in the second of these directions to

an end position, then the end of the electrode will generally extend further beyond the end position of the beam centre than in an electrode produced with a 90° deposition angle. This direction can be on the line of intersection between a plane and the surface of the substrate, the plane being perpendicular to the substrate and parallel to the electron beam. It will be appreciated that, for any given gap between the end points of the template lines for a pair of nanoelectrodes, the actual gap size and shape produced will depend on the deposition angle. This can be used to produce a pair of nanoelectrodes with an actual gap size that is smaller than the nominal resolution of the SEM. It can also result, as shown in Figure 2b, in a nanoelectrode shape that is narrower, sharper and more pointed at the electrode tip than those produced with a 90° deposition angle.

The additional Pt contact pads 23 (250 x 500 nm) were deposited by EBID to improve electrical connection to the Au microelectrodes.

We have fabricated 126 junctions (nanoelectrode gaps) with a nanopore. Inhomogeneity of the substrate surface, sample charging and stage drift gave rise to an uncertainty in the localization of the nanogap relative to the nanopore in some devices. The electrode gap was precisely aligned with the nanopore in 60% of the devices. Out of these, 20% exhibited tunnelling characteristics that were stable and reproducible over several days. These devices were then used for DNA translocation experiments. For comparison, we also performed tunnelling spectroscopy experiments on devices where the electrode gap was not aligned to the nanopore in order to verify that the presence of the pore does not affect the tunnelling characteristics.

In a control experiment, we determined the (ionic) conductance of the device before and after Pt electrode deposition. If the electrode junction is precisely aligned with the nanopore and the gap size is smaller than the pore diameter, a significant decrease in the pore conductance would be expected. This is experimentally observed and shown in Figures 3 and 4 for a representative set of devices.

Figure 3 shows representative ion current vs. bias voltage plots before and after electrode deposition, including SEM images of the respective device (insets). The pore conductance G, as determined from the slope of these traces, decreases from 71.6 ± 0.1 nS to 6.0 ± 0.1 nS. For the device before electrode deposition, G is in good

agreement with the calculated value using equation (1) based on the geometrical dimensions of the pore (obtained from SEM imaging and the thickness of the membrane), which yields 52 ± 15 nS. The relatively large error of the latter emerges from the uncertainty in the pore diameter and membrane thickness.

$$G = \frac{\pi}{4}\frac{d_{pore}^2}{L_{pore}}\left((\mu_K + \mu_{Cl})n_{KCl}e + \mu_K\frac{4\sigma}{d_{pore}}\right) \quad (1)$$

where d_{pore} is the (effective) pore diameter; L_{pore} the (effective) length of the pore, μ_K and μ_{Cl} are the electrophoretic mobilities of K+ and Cl-, respectively; n_{KCl} is the number density of the electrolyte, e the elementary charge and σ is the surface charge density in the nanopore.

Since equation (1) is strictly only valid for cylindrical pores with a high aspect ratio, it cannot provide reliable estimates of G for devices after electrode deposition due to the rather complex geometry. Rather, we use eq. (1) and the experimentally determined value of G to estimate the effective pore diameter. Neglecting the surface contribution to G due to the high electrolyte concentrations used, we rearrange eq. (1) and obtain:

$$d_{pore} \approx \left(\frac{4GL_{pore}}{\pi(\mu_K + \mu_{Cl})n_{KCl}e}\right)^{\frac{1}{2}} \quad (2)$$

A comparison of the calculated effective pore diameter determined using eq. (2) is shown in Figure 4 for a total of 10 representative devices. Devices 1-5 do not have Pt nanogaps. The calculated pore diameters range from 50-80 nm (green circles) and compare well with values obtained by SEM imaging (black squares). A further set of devices (6-10) with Pt nanogaps exhibits significantly reduced pore diameters typically well below 10 nm (5 – 18 nm). Qualitatively, these values are in line with what was observed in SEM images.

After electrode deposition, the next step in the fabrication process was to ascertain that the tunnelling junction is functional. To this end, we performed *I-V* tunnelling spectroscopy in a range of different solvents with different tunnelling barriers (air, 0.1 M NaClO4, *n*-hexane and dimethylsulfoxide (DMSO)). The resulting *I-V* spectra were fit according to the Simmons model, eq. (3), in the low-bias regime (Vbias << Φ_B). This is a reasonable approximation since the tunnelling barrier for water-filled junctions has been reported to be on the order of 1 eV whereas we considered a bias range between +/-0.3 V. For each junction, multiple *I-V* curves were recorded at a scan rate of 0.02 V/s.

$$I = A\left(\frac{e}{4\pi^2 \hbar d^2}\right)\left\{\left[\left(\Phi_B - \frac{eV}{2}\right)\exp\left[-\frac{2(2m)^{\frac{1}{2}}}{\hbar}\left(\Phi_B - \frac{eV}{2}\right)^{\frac{1}{2}} d\right]\right] - \left[\left(\Phi_B + \frac{eV}{2}\right)\exp\left[-\frac{2(2m)^{\frac{1}{2}}}{\hbar}\left(\Phi_B + \frac{eV}{2}\right)^{\frac{1}{2}} d\right]\right]\right\} + B \quad (3)$$

d is the gap distance, Φ_B is the effective tunnelling barrier height, *A* the active tunnelling area and *B* is a parameter that takes into account any current offset at zero bias (due to residual Faradaic processes or minor calibration errors).

At first, we compare different devices (with different gap sizes) in the same medium (i.e. constant barrier height). Figure 5 shows *I-V* curves in 0.1 M NaClO4 for six typical Pt nanogap devices and two controls: a device with Au microelectrodes separated by a 2 μm gap (control 1) and one with a single Pt nanowire bridging both Au microelectrodes (same deposition conditions as the gaps, control 2). The *I-V* curves for the Pt nanogap devices are non-linear (in accordance with eq. (3)) with current levels significantly higher than in control 1 (0.01 nS) and lower than in control 2 (420 nS). For tunnelling junctions deposited with nominal gaps sizes between 50 – 60 nm, we measured tunnelling conductance in the range of 0.2 – 4 nS.

We fit the *I-V* curves according to eq. (3) in order to extract the electrode gap size and tunnelling barrier. For 0.1 M NaClO4, these parameters were determined to be between 1.6-2.2 nm and 0.69 ± 0.27 eV respectively. Importantly, the barrier height was in good agreement with previously reported values obtained by electrochemical STM. Additionally, the measured tunnelling currents and the corresponding calculated gap distances compare well with results previously reported for tunnelling gaps fabricated with variable gap distance.

Previously, non-linear *I-V* curves have been reported for Pt nanowires fabricated by EBID and rationalized by electron tunnelling between Pt crystallites. In order to discriminate from this case and to confirm that we have fabricated functional tunnelling junctions we performed *I-V* spectroscopy for the tunnelling junctions in different solvents (i.e. with different barrier heights).

Tunnelling barriers for hexane, DMSO, and water have been reported to be 3.46 eV, 2.12 eV, 0.93 eV respectively. The barrier height for air has been reported to range from 0.7 – 4.7 eV depending on the local environment. According to eq. (3) such variations translate into significant differences in the tunnelling current. On the other hand, in the case of a single nanowire, the measured current is expected to show little variation with the solvent, since its conductivity is dominated by the nanowire material.

For devices fabricated with a nanogap (Figure 6a-c), we observed significant, but reproducible variation in the *I-V* curves, depending on the solvent used. It should be noted that we randomized the sequence of solvents, in order to exclude any interference from cross-contamination. Effective barrier heights were calculated to be 0.69 ± 0.27 eV for 0.1 M NaClO4, 2.07 ± 0.64 eV in DMSO, and 3.32 ± 0.78 eV in *n*-hexane. All these values are in good agreement with the literature (see above). In air, we observed a relatively low barrier height of 1.35 ±0.52 eV, which is likely due to vapor condensation in the gap. For control 2 (Pt nanowire, no gap), under the same experimental conditions, solvent dependence was not observed (Figure 4d), which confirms that we can distinguish functional tunnelling junctions from short-circuited and other dysfunctional devices.

Fully characterized devices exhibiting tunnelling behavior were then used to perform DNA translocation experiments. Simultaneous measurement of tunnelling and ionic currents was carried out by combining a Gamry Reference 600 potentiostat (tunnelling current measurements, 5 kHz acquisition frequency, no filter) and an Axopatch 200B patch-clamp amplifier (ionic current measurements, 50 kHz acquisition, 5 kHz Bessel filter). The nanopore/nanogap device was packaged in a glass flow cell with two reservoirs filled with 1 M KCl, 10 mM Tris-HCl 1mM EDTA. Ag/AgCl electrodes were inserted in each reservoir and connected to the Axopatch amplifier. The Ag/AgCl electrode in the top reservoir was used as common ground for both the Axopatch and

Gamry instruments. λ–DNA (48.5 kbp, 10 μg/ml) was added to the bottom reservoir (opposite to the tunnelling gap, as shown in Figure 1a) in order to minimize spontaneous adsorption of DNA molecules to the electrode gap. In this configuration, the DNA must translocate through the pore in order to reach the tunnelling junction. For translocation experiments, a bias voltage, Ei = -0.8 V, was applied to the Ag/AgCl electrodes. The bias voltage across the tunnelling junction was set to Et = 0.3 V.

Typical ion current-time (black) and tunnelling current-time (gray) traces are shown in Figure 7. Note that ionic current (black curves) is always negative and that events occurring upward decrease the nanopore conductance. Acquisition frequency: 50 kHz for ionic current, 5 kHz Bessel filter; 5 kHz for tunnelling, no filter. (a) Ionic current for short lived type I events. (b) Tunnelling current for long lived Type II events. (c) Examples of coincident type II events detected in both detection channels.

We have performed statistical analysis on a total of 3429 events and observed two classes of events: short-lived transients (type I) and longer lived events (type II). Type I events exhibited a mean dwell time τ of 0.3 ± 0.2 ms and a mean amplitude of 2.5 ± 0.7 nA. They formed the majority of the observed events; a typical section of the ion current-time trace is shown in Figure 7a. With the extended length of λ-DNA being 16.5 μm, this translates into a translocation speed of 5.5 cm/s. Importantly this is in excellent agreement with previous results which reported translocation speeds between approximately 2 and 6 cm/s, depending on the bias voltage at a membrane thickness of ~10 nm. For a proper quantitative comparison, the respective values should be corrected for the actual electric driving field. However, with the geometry of our electrode/nanopore device being rather complex, we can only estimate its magnitude. Taking the nominal thickness of the Si_3N_4 membrane of 70 nm as a reference, we obtain a value of 0.8 V/ $70x10^{-9}$ m = $1.1x10^7$ V/m, which is somewhat smaller than the values given by Chen et al. (ca. $2x10^7$ to $6x10^7$ V/m). Since the tunnelling junction represents a significant constriction in the pore (and thus a source of resistance), the effective membrane thickness is likely to be smaller than 70 nm, resulting in a larger local electric field. Based on the translocation speed observed in our experiments and comparison with previously reported data, we are confident that the type I events are actually DNA translocation events. “Bumping events”, i.e. ion current blockades that originate from DNA colliding with the pore entrance without

actually entering the pore, are expected to be even faster than the type I events and were not detected in our experiments.

It should also be stated that these events were not detected when measuring the tunnelling current. This could have several reasons: First, the tunnelling data are recorded at a rate of 5 kHz (200 μs); therefore, the short lived type I events are most likely too fast to be recorded. Unfortunately, in the present configuration faster acquisition rates were not possible. In further studies, we intend to modify the electronics to perform tunnelling experiments at the same acquisition rate as that of the ionic current (50 KHz). Secondly, tunnelling current modulation could be too small to be detected in the current experimental configuration.

Previous work has shown tunnelling current modulation due to individual bases of ~ 10 pA. If these values are also representative for tunnelling current modulations for a DNA strand in the present configuration, such small variations are most likely embedded in the tunnelling current noise, which is currently on the order of 1 nA, cf. Figure 7. Finally, since the tunnelling-active area is smaller than the cross-sectional area of the pore, there is a non-zero probability that DNA strands actually by-pass the tunnelling junction. The ratio of by-passing DNA and DNA detected by the tunnelling junction depends on the device design and can, in principle, be optimized. Interestingly, by-passing DNA would experience a larger constriction and translocate much faster than DNA going through the much narrower tunnelling junction. In the latter, the DNA is also more likely to undergo structural changes, such as (partial) unzipping, to temporarily clog the pore and/or adsorb to the metal surface.

In accordance with this picture, we also observed longer-liver events (type II) with characteristic dwell times between 1.5 and 200 ms (Figure 7b). These events were recorded in both the tunnelling and ionic current data. A total of 108 type II translocation events were detected. The mean dwell time and amplitude of the tunnelling events was 4.7 ms ± 4.3 ms and 3.7 ± 0.4 nA respectively. The increase in the tunnelling current upon DNA translocation is in accordance with STM imaging data of DNA. The signals obtained in our experiments were higher, which could be due to the DNA/electrode coupling being stronger (stronger electronic overlap or multiple bases conducting in parallel). The dwell times for type II events were on average 16 times longer than for type I events. Previous similar observations state that

non-specific binding between the DNA and the nanoelectrodes could be used to explain the spread over time. This is likely the case in our experiments and would explain the wide dwell time distribution.

Importantly the dwell time for the tunnelling current compares well with that detected for the ionic current (Figure 7c). The ionic current had a mean dwell time τ of 6.3 ± 3.2 ms and mean amplitude of 7.0 ± 1.8 nA. The lower translocations times observed with the tunnelling data are due to the DNA leaving the tunnelling junction prior to the pore being fully unblocked. Furthermore, a small fraction of the type II events (20%) had a signal in either of the ionic current or tunnelling traces, which is likely due to adsorption or bumping of the DNA on either the electrode without any translocations taking place.

In a further embodiment a single device with multiple pores in a single substrate is produced. This device is essentially the same as that of Figure 1a, except that multiple pores, each with a respective pair of electrodes, are all formed in the substrate membrane. Several nanopores can be formed over a single micropore or etched cavity in the silicon layer, or several micropores can be formed and a single nanopore, or multiple, nanopores formed over each one. In this embodiment the device can be formed on the same multibeam system of Figure 2a, but the controller is programmed to form the separate nanopores in suitable positions by controlling the direction of the ion beam during milling of the nanopores, and then to form the electrode pairs for each nanopore. Alternatively the ion beam can be left in the same direction for all the nanopores, and the substrate moved by controlled movement of the sample table to control the positions of the nanopores in the substrate.

Devices with more than two electrodes around a nanopore can be fabricated in the same way. It will be appreciated that if there are three, or four, electrodes spaced around a nanopore, then the gap between them can be controlled by varying the deposition angle of one or more of the electrodes.

It will be appreciated that various aspects of the embodiments described above can be varied. For example, the substrate can be supported in other ways rather than being supported over a cavity or micropore in a support material. Different materials can be used for the substrate and the electrodes. The substrate can be of any suitable non-

conductive material (e.g. Si_3N_4, SiO_2 or SiC or polymeric membrane materials such as Poly(ethylene terephthalate)). The nanoelectrodes can be formed of other conductive materials such as gold, silver or tungsten. The dimensions of the device can be varied depending on the exact application for which it is intended. Furthermore the device can be fabricated using different methods, for example FIB deposition can be used instead of EBID. Also separate systems, or other multibeam systems, can be used for forming the nanopore and forming the electrodes rather than using a dual beam system. Other modifications and variations will be apparent to those skilled in the art.

Claims

1. A method of fabricating a nanopore device, the method comprising: providing a layer of substrate material having a pore through it, and depositing a pair of electrodes on the surface of the substrate material such that the electrodes are located adjacent to the pore, wherein the electrodes are deposited by particle beam induced deposition.

2. A method according to claim 1 wherein at least one of the electrodes is deposited so as to partially block the pore.

3. A method according to claim 1 or claim 2 wherein the pore has a mean diameter of 100nm or less.

4. A method according to any foregoing claim wherein the electrodes are deposited so as to leave a gap between them of 10nm or less.

5. A method according to any foregoing claim wherein the deposition is induced using a particle beam that is non-perpendicular to the surface of the substrate.

6. A method according to claim 5 wherein the deposition is induced using a particle beam that is at a deposition angle of 80° or less to the surface of the substrate.

7. A method according to claim 5 or claim 6 wherein during the deposition the particle beam is moved along the substrate in a direction which is non-perpendicular to the beam.

8. A method according to claim 7 wherein the beam is moved along the substrate in a direction that is on the line of intersection between a plane and the surface of the substrate, the plane being perpendicular to the substrate and parallel to the particle beam.

9. A method according to any foregoing claim wherein the pore is formed by a particle beam.

10. A method according to claim 9 wherein the pore and the electrodes are formed by respective beams of a multibeam apparatus having two particle sources each arranged to direct one of the beams at the substrate.

11. A method according to any foregoing claim wherein the pore is one of an array of pores formed through the substrate, and a pair of electrodes is formed adjacent to each of the array of pores.

12. A nanopore device comprising a substrate having a pore through it, and a pair of electrodes formed on the substrate and located adjacent to the pore, wherein the electrodes comprise nanowires formed on the surface of the substrate.

13. A device according to claim 12 wherein the electrodes define a gap between them of no more than 10nm.

14. A device according to claim 13 wherein the electrodes define a gap between them of no more than 5nm.

15. A device according to any of claims 12 to 14 wherein at least one of the electrodes partially blocks the pore.

16. A device according to any of claims 12 to 15 wherein the electrodes are located on opposite sides of the pore.

17. A device according to any of claims 12 to 16 wherein the pore is one of an array of pores through the substrate, each pore of the array having a respective pair of electrodes adjacent to it.

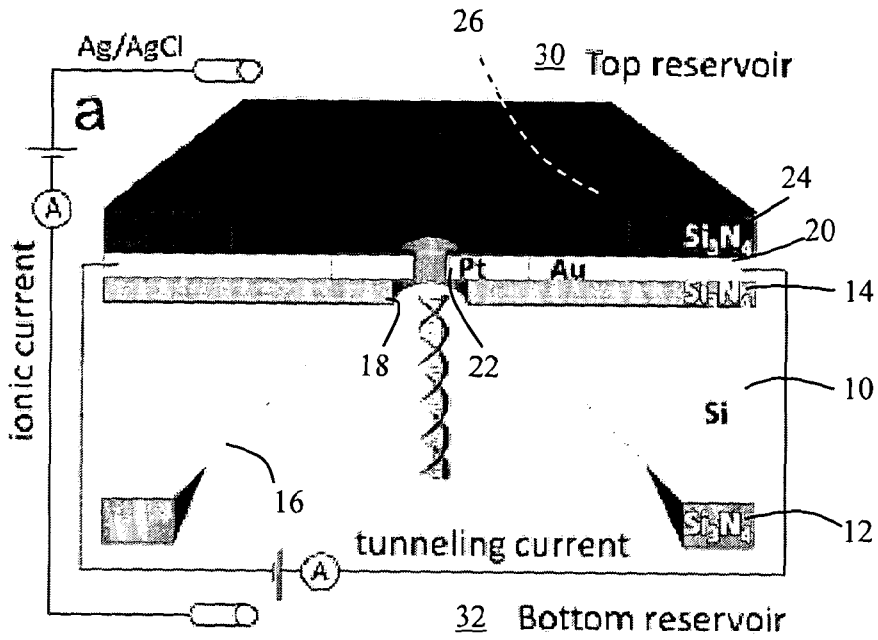

Fig. 1a

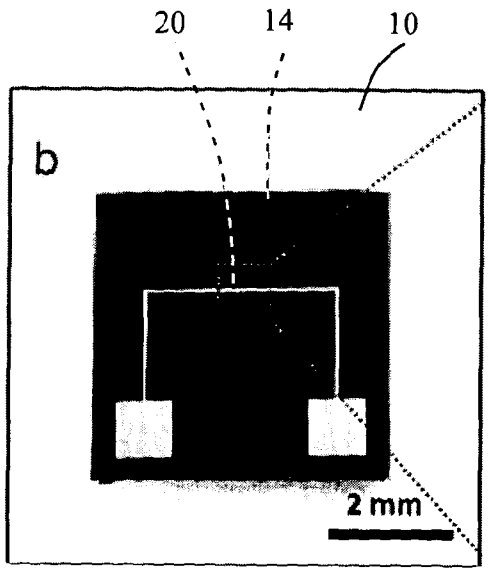

Fig. 1b

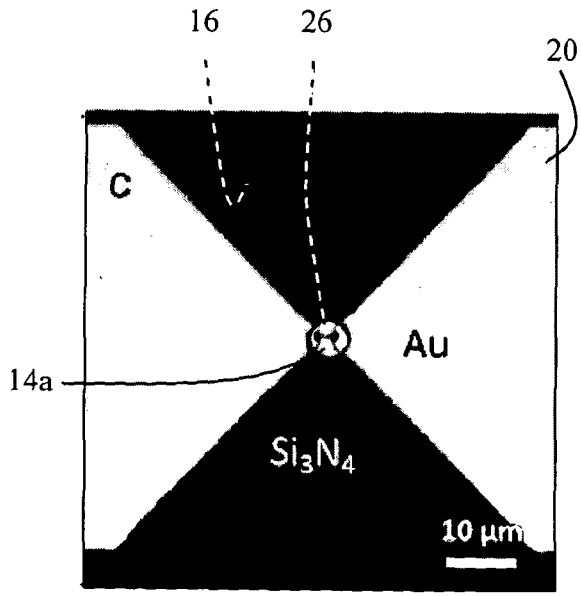

Fig. 1c

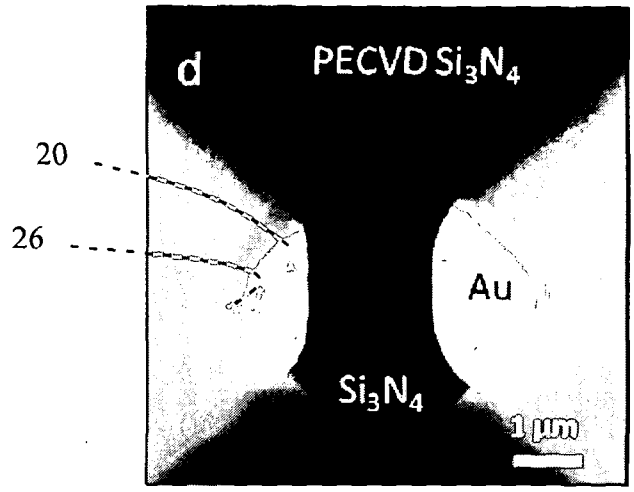

Fig. 1d

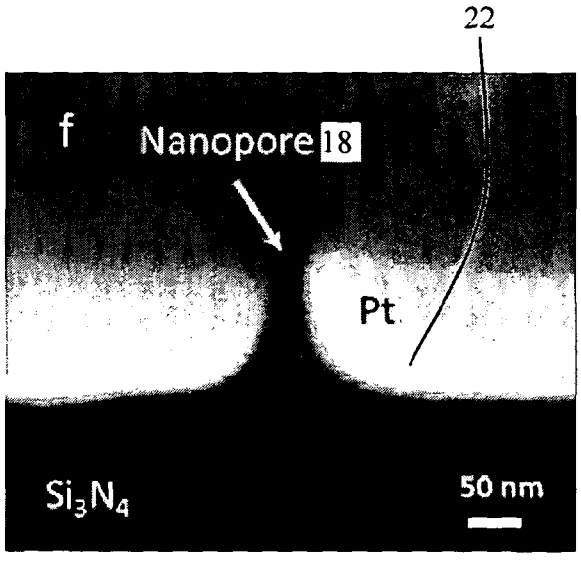

Fig. 1f

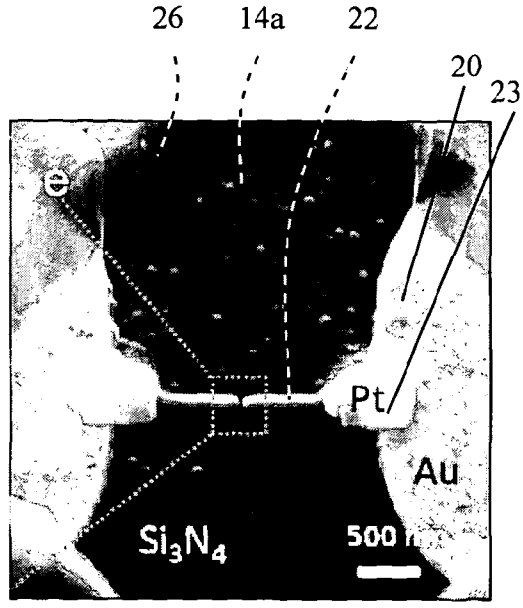

Fig. 1e

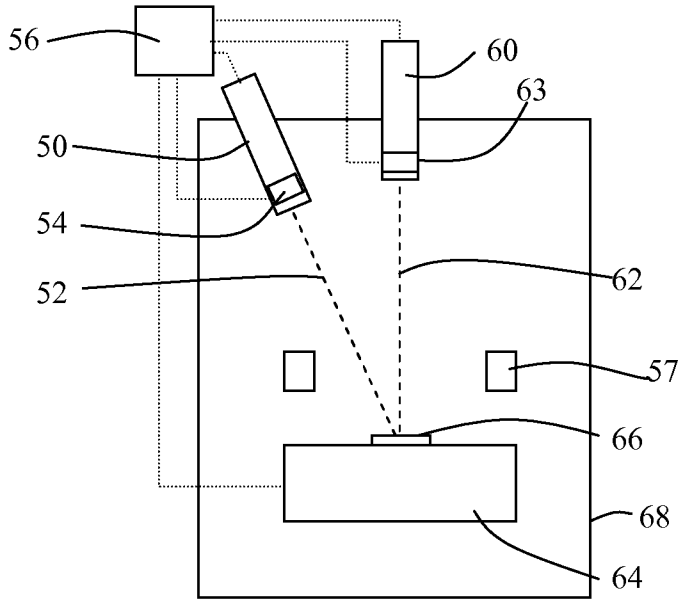

Fig. 2a

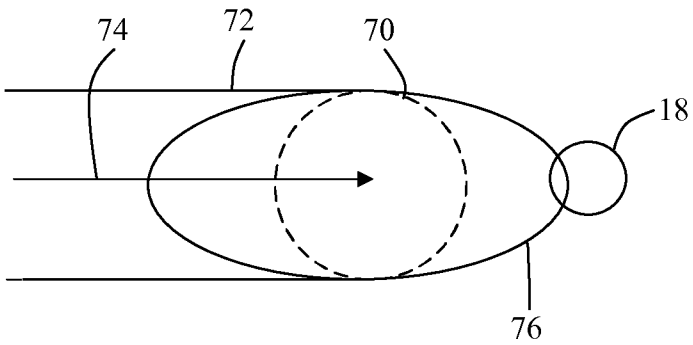

Fig. 2b

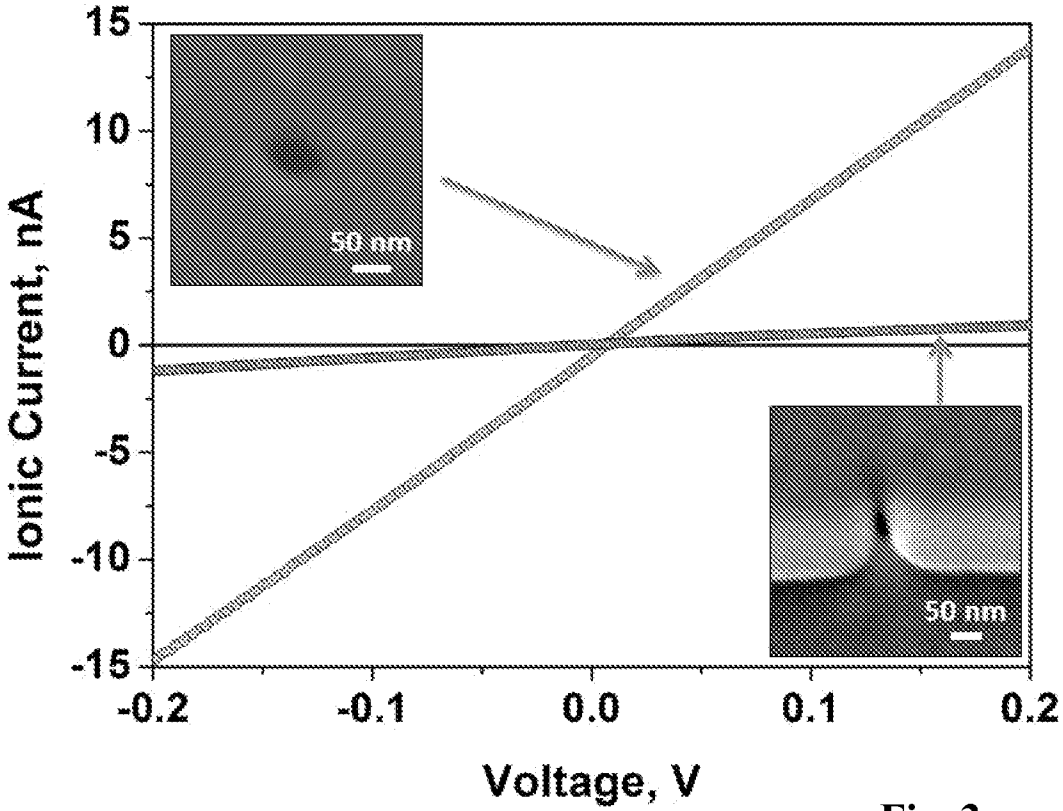
15
10
5
0
-5
-10
-15
-0.2
-0.1
0.0
0.1
0.2
Ionic Current, nA
Voltage, V
50 nm
50 nm

Fig. 3

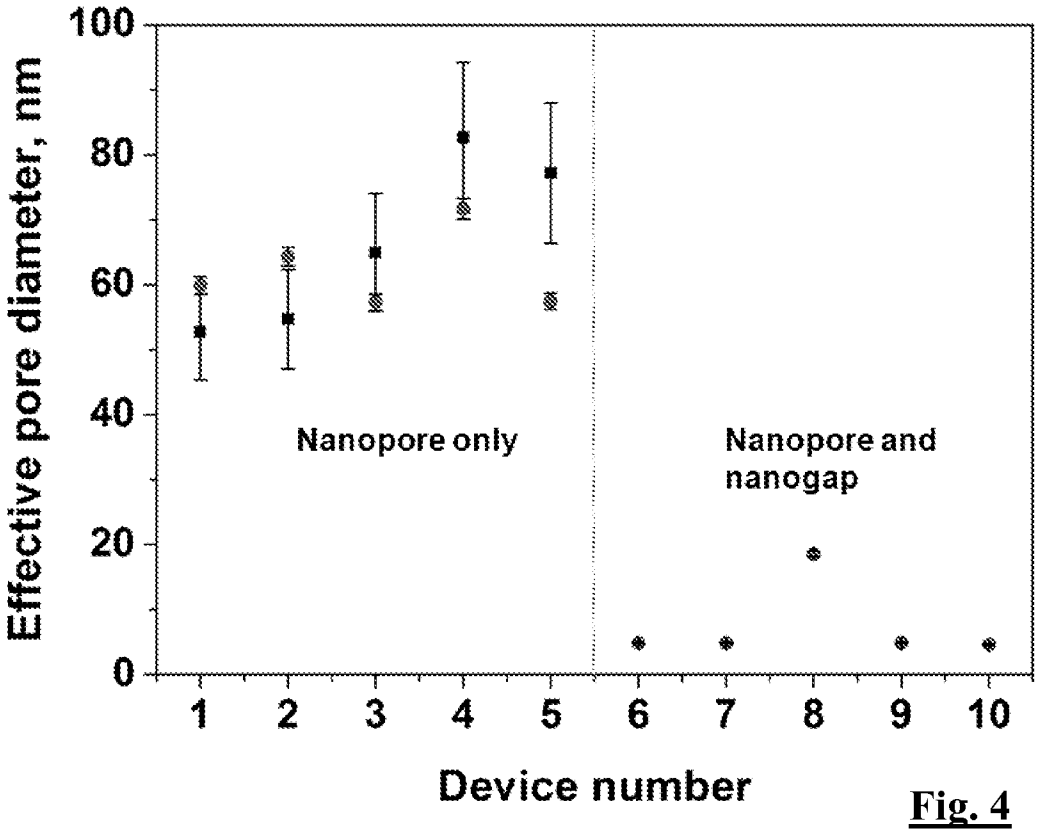
Effective pore diameter, nm
100
80
60
40
20
0
1
2
3
4
5
6
7
8
9
10
Device number
Nanopore only
Nanopore and
nanogap

Fig. 4

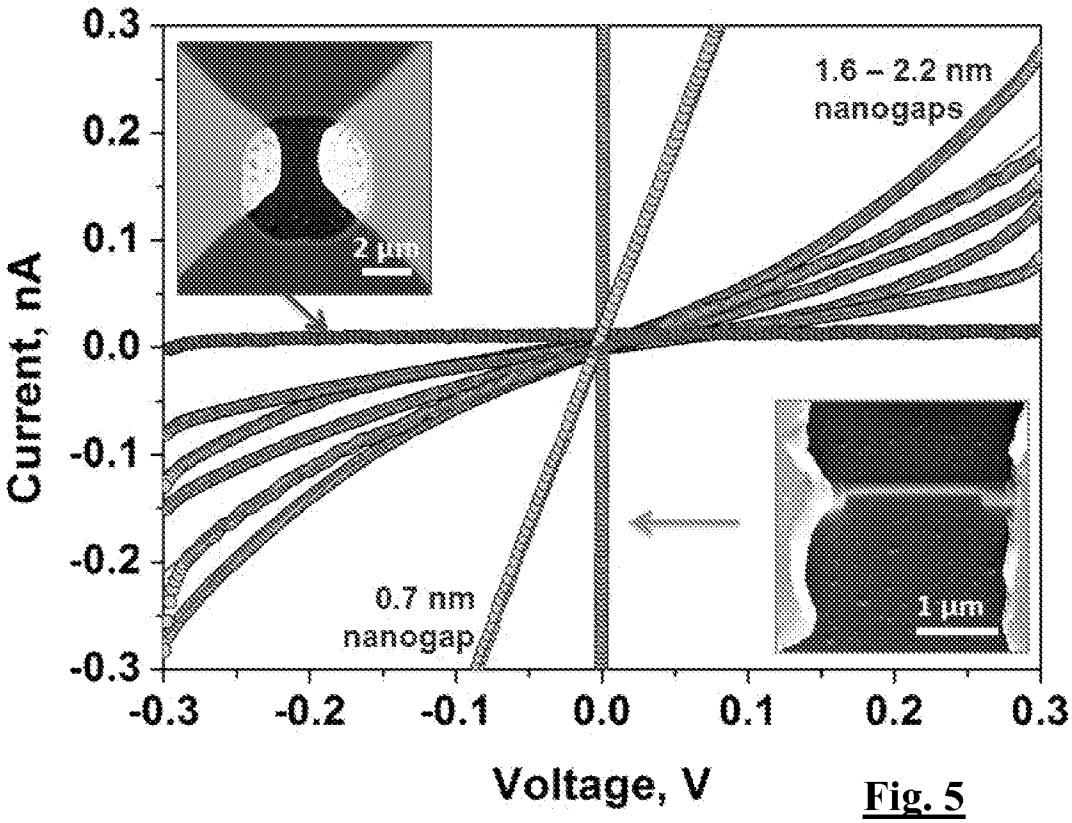
Current, nA
0.3
0.2
0.1
0.0
-0.1
-0.2
-0.3
-0.3
-0.2
-0.1
0.0
0.1
0.2
0.3
Voltage, V
1.6 – 2.2 nm
nanogaps
2 μm
0.7 nm
nanogap
1 μm

Fig. 5

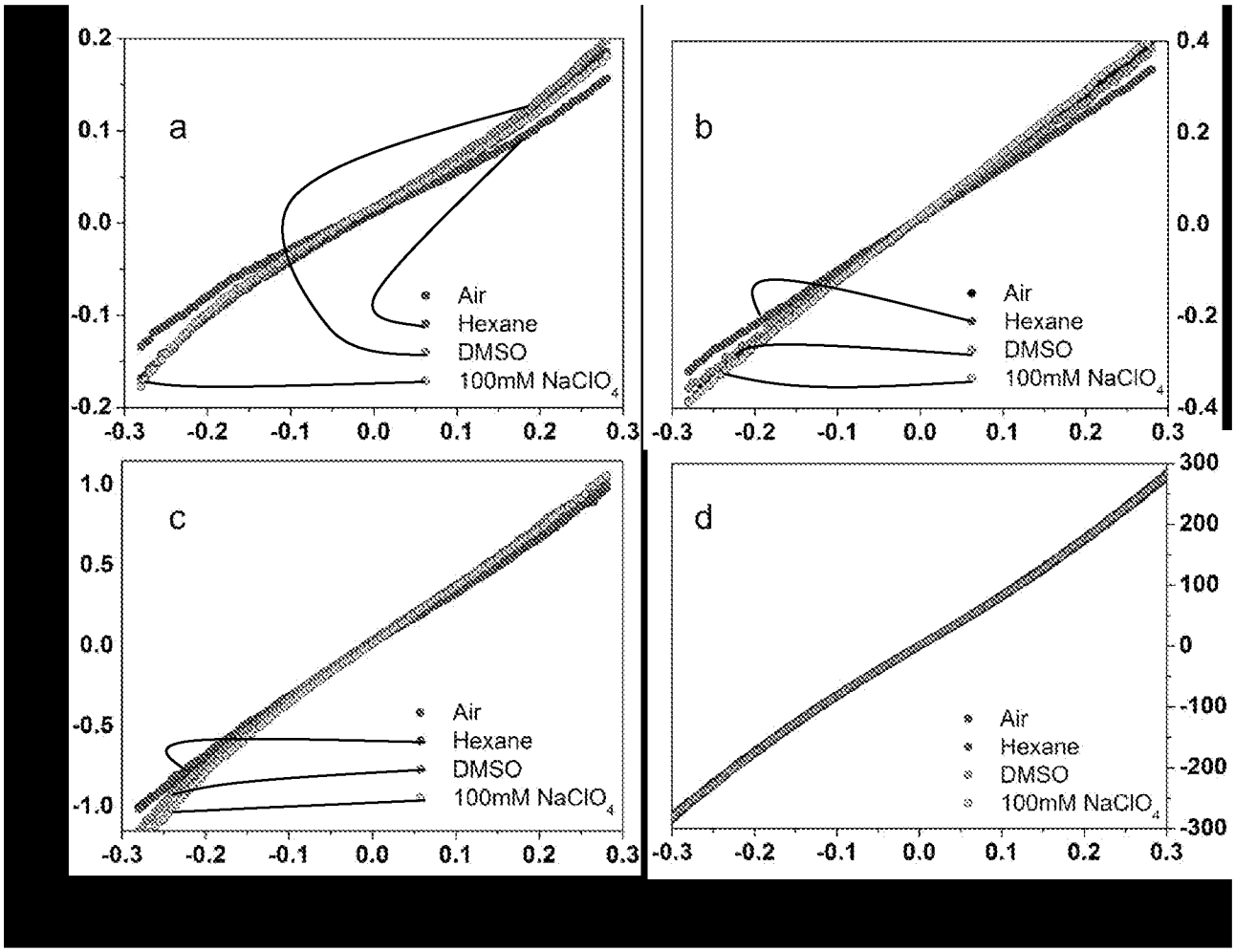
a
Air
Hexane
DMSO
100mM NaClO4
b
Air
Hexane
DMSO
100mM NaClO4
c
Air
Hexane
DMSO
100mM NaClO4
d
Air
Hexane
DMSO
100mM NaClO4

Fig. 6

Ionic current
Tunneling current

Fig. 7